

# METHODOLOGY FOR PRESS FORMING SIMULATION OF A CONTINUOUS FIBER-REINFORCED POLYMER COMPOSITE

Bressan, Fabio<sup>1</sup>; Jovas, Bob<sup>2</sup>; Luchini, Timothy<sup>3</sup>; Rodriguez, Alejandro<sup>1</sup>; Rogers, Scott<sup>1</sup>; Russell, Richard<sup>2</sup>; Hahn Gail<sup>3</sup>

<sup>1</sup>Solvay Composite Materials, Anaheim, CA 92806

<sup>2</sup>Solvay Composite Materials, Heanor, UK

<sup>3</sup>The Boeing Company, Saint Louis, MO 63134

## ABSTRACT

Numerical simulation is a powerful tool in manufacturing since it provides a lower cost and faster analysis than actual trial-and-error testing. Press forming manufacturing simulation can be realized with many different system configurations including different boundary conditions and material set up. This work presents numerical analysis, advanced material card development and validation of a real component manufactured through press forming using thermoset prepreg material. The simulation was performed with an explicit numerical code and is visually correlated with a final experimental results.

Corresponding author: Gail Hahn

## 1. INTRODUCTION

Press forming of CFRP parts provides high rate, repeatability and cost reduction when coupled with mass production techniques in industrial and aerospace applications. Simulation of the part-forming process using an FEM numerical approach is an effective method to predict defects and facilitate the design for manufacturing [1-11].

The aim of this project is to evaluate the state of the art of simulation with traditional general purpose and specialized software present in the market. The software analysis requires the properties of the material to be represented by a software material card.

The high deformability of the thermoset composite pre-preg material at expected molding temperature was characterized by Purdue University laboratories and the material card was developed within the Solvay Virtual Engineering Team.

A manufacturing simulation analysis was performed for two different part geometries: a beaded panel representative of a geometrically stiffened structures and a C-frame part representative of a structural geometry. In particular for the beaded panel, the prediction capability was evaluated with a visual correlation to the real experimental manufacturing process.

The limits and the advantages of using a numerical method to predict some of the defects in the experimental test was evaluated with a preliminary experimental correlation analysis.

## 1.1 Press prepreg manufacturing process

Press manufacturing of parts from continuous fiber-reinforced thermoset composites has been specifically developed for high volume aero and automotive applications. Fast cure cycles and compatibility with automated processes (robots) are important to the press forming process.

Figure 1 shows the process flow for a part manufactured through compression molding. The first step of the process is to prepare the 2D flat blank; this step encompasses the cutting and kitting of the plies, ply collation by pick & place or hand layup followed by a RT debulk. After blank preparation the blank is loaded on the spring frame and loaded onto the press for processing. The blank is then shuttled to the IR preheat station where it resides for a short period of time before being moved into the tool on the press where it is formed and consolidated. Further details are shown in [12].

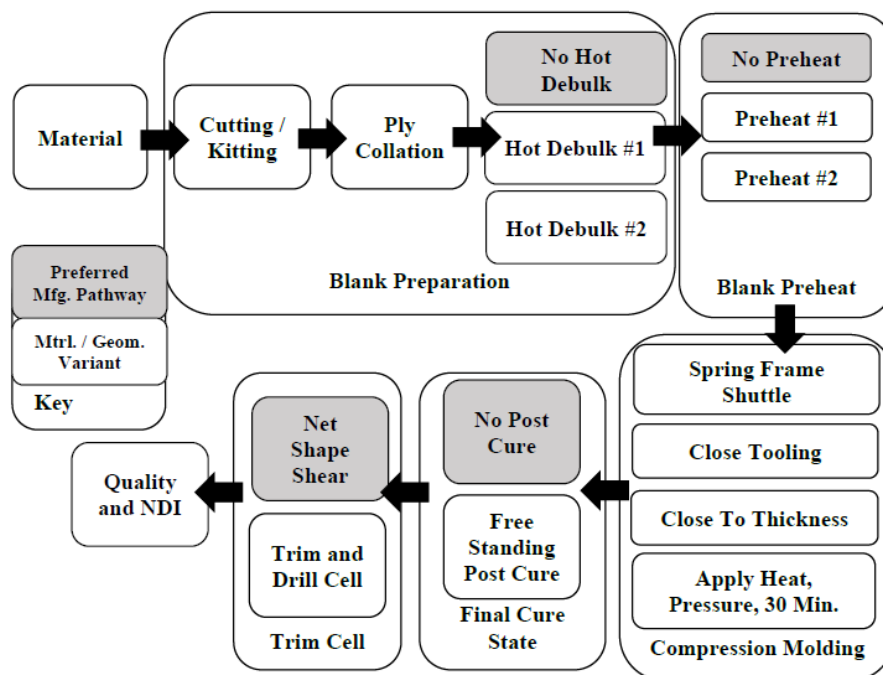
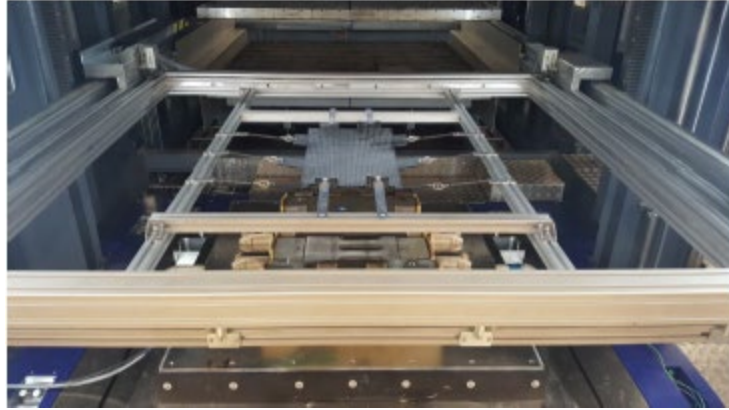


Figure 1. Simplified spring frame compression molding process for aerospace capable composite parts [12]



*Figure 2. Beaded panel blank loaded into the spring frame ready to be shuttled into the preheat station [12]*

Press tools are more expensive than a typical hand layup approach and simulation of the forming process before tool machining verifies both the design parameters and allows exploration of the optimum layup for a new component.

## **1.2 State of the Art of Press Forming Simulation**

During the preliminary stage of this work, different commercial numerical codes were evaluated. The main evaluation criteria considered were primarily the accuracy, secondarily the speed of the codes, and finally the quality of the material models implemented (material cards definition).

Most of the general purpose finite elements commercial codes are well established in the metals industry. The software solvers are calibrated and predictive with material cards for homogenous materials. The automotive industry uses forming simulation mainly for sheet metal for external panels. Forming simulation for metal can predict the residual stress in the part which allows the designer to optimize thickness, reduce waste and improve the overall process for manufacturing. Forming simulation for complex shapes is currently solved with the implementation of explicit commercial computer codes. This numerical solution is fast and accurate in predicting wrinkling and improving the design for manufacturing of new geometries.

The three major challenges for any numerical simulation for manufacturing are:

1. Thermoset materials requires a special material card that need to take into account the interdependence between viscosity and temperature. Different than Thermoplastic, Thermoset materials are not reversible [7].
2. Material card is mesh dependent.
3. The prediction of the wrinkling and fiber direction for complex geometries requires an explicit code. Implicit solvers are not fast enough with very fine mesh. Implicit solvers can't solve multiple contacts between layers.

For this specific project the solution proposed was performed by Ls-dyna explicit code because it was the technology, at that time, which provided an excellent material card and a good compromise of speed and accuracy. Hypermesh and Lsprepost were used for pre and post definition and J-composites was used for auto/semi-auto processing material card from the experimental tests.

Additional tools were integrated in the process of simulation in order to develop an accurate material card from the experimental test log files. In particular J-sol form J-composite. It was also possible to develop specific TCL (Altair) scripts to accelerate the time consuming preprocessor procedure. LaminateTools (from Anaglyph) was the tools used for generating flat pattern of each single layers.

## 2. EXPERIMENTATION

### 2.1 Solvay Material Characterization of CYCOM® 5320-1 prepreg

Solvay CYCOM® 5320-1 prepreg was characterized at forming temperature of 370 F after being pre-consolidated. The textile used was a T650-35 3K 8HS at 370 gsm for the generation of the material cards using LS-DYNA solver.

### 2.2 Cure Cycle

All material samples were characterized and tested in accordance with the temperature cycle specified in Figure 3. Temperature was maintained as close as possible to the profile with the test beginning at the region labeled as “Forming 1”. Test speeds were chosen to make sure tests finished in less than 30 seconds to ensure that there wasn’t a significant property change developed during the test. The environmental chamber used to conduct the high temperature tests is shown in Figure 4. The actual temperature data vs. the target temperature data is shown in Figure 5. As the figure shows, the oven was able to track the temperature closely except at the very end where it was not quite able to keep up with the desired heating rate. Some tests were started at around 125 F (as shown) due a lack of oven cooling and the delay in cooling to room temperature [2].

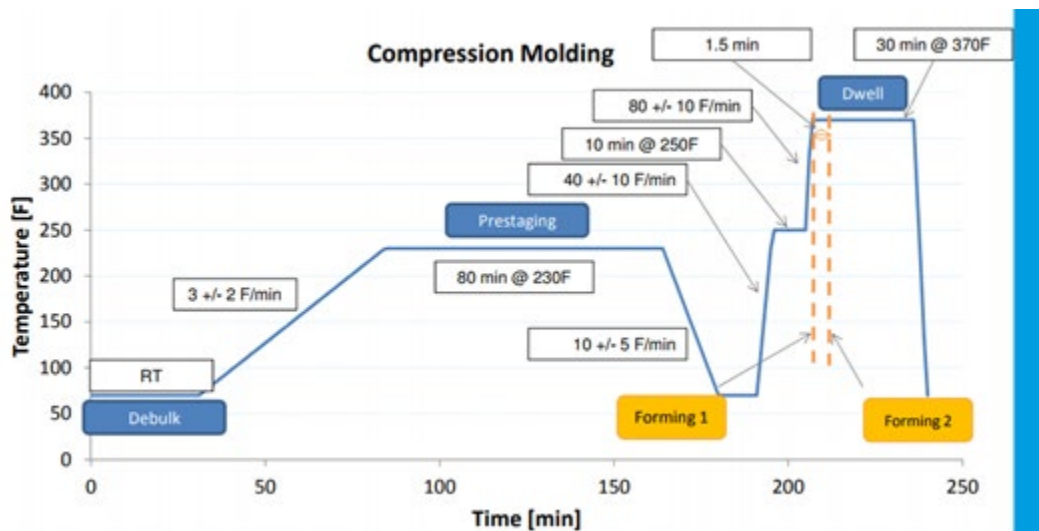


Figure 3. Temperature cycle used for characterization of the mechanical properties of CYCOM® 5320-1 3K 8HS prepreg.



Figure 4. Temperature chamber used to characterize the prepreg material at forming temperature.

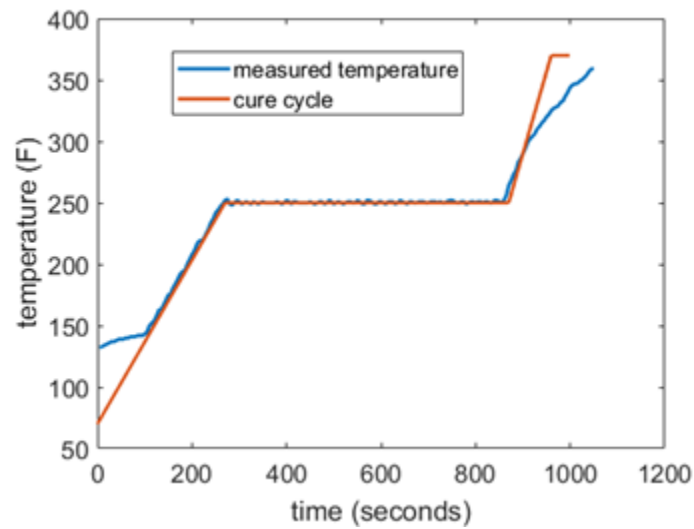
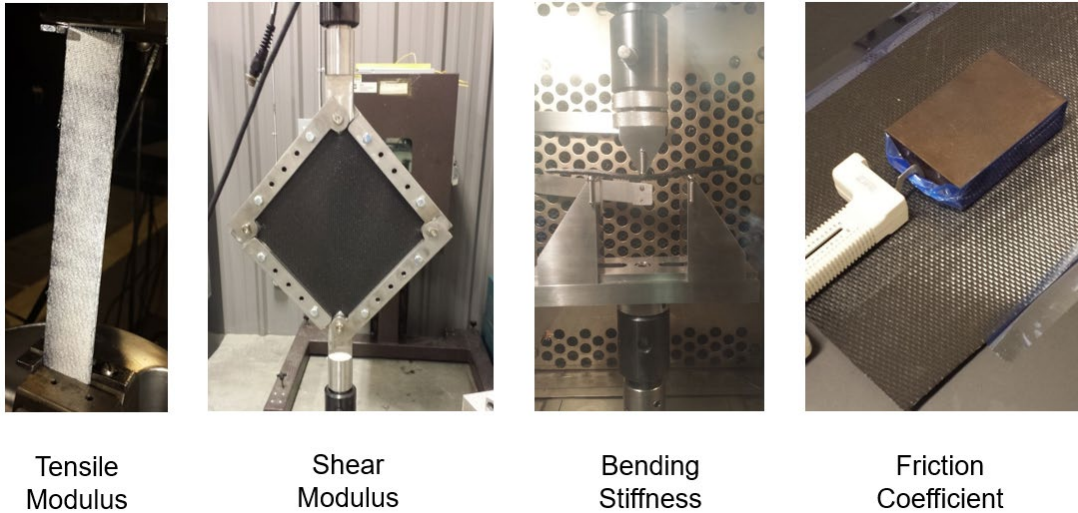


Figure 5. Target temperature vs. logged temperature during the characterization of the prepreg material.

#### Tensile Modulus, Shear Modulus, Bending Stiffness and Friction Coefficient

In order to generate the material card for any commercial solvers, it is necessary to perform a minimum of four fundamental tests as shown in Figure 6.



*Figure 6. Tests performed for tensile modulus, shear modulus, bending stiffness, and friction coefficient tests.*

### **2.2.1 Tensile Modulus**

The tensile modulus measurements were attempted at high temperature. However, in order to accurately measure modulus there must be a way to verify strain in the sample. Typically this is done either by attaching a strain gauge to the sample or by using digital image correlation (DIC). Unfortunately, because neither strain gauging nor DIC was able to be successfully performed, the room temperature tensile modulus was assumed to be roughly equal to the high temperature tensile modulus. Tensile modulus is dominated by the fiber modulus and the assumption was that the final property of 3.1 GPa tested for room temperature was an accurate estimation for the numerical simulation.

### **2.2.2 Bending Stiffness (Flexural Modulus)**

The flexural modulus was measured according to the standard ASTM D7264 in the 3 point bend configuration. Figure 7 shows the test setup for the flexural modulus results. The span length of the sample was 78 mm. The width was 25.4 mm and the thickness was 2.6 mm. The machine head rate was set at 10 mm per minute. The force displacement curves and the stress strain curves were then generated [4]. The modulus was estimated using the data up to 1% strain. The flexural modulus was calculated to be 9.7 MPa.



Figure 7. 3-point bending test set-up.

### 2.2.3 In plane Shear Modulus

The in-plane shear modulus of the prepreg was measured using a picture frame test [1]. Figure 8 shows the picture frame test setup before beginning the test and as it nears completion. The force and displacement are measured by the load frame and are converted into shear force and shear strain to get the shear modulus of the material. The machine was pulled at 3 mm per second and the length of each side of the picture frame fixture is 190 mm. Figure 8 (right) shows the force-shear angle curves.

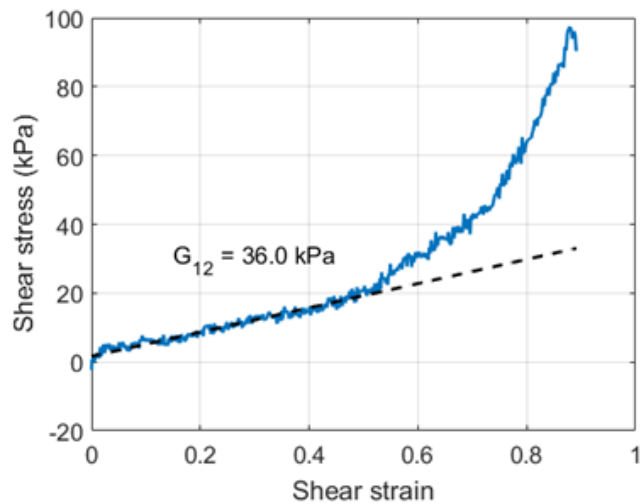
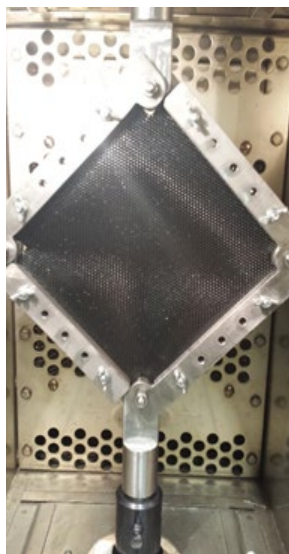


Figure 8. Left: Picture frame test setup. Right: Shear modulus estimation based on data log.

The shear modulus is calculated using the initial flat slope of the shear stress-shear strain curve. Figure 7 shows an example of the shear modulus being estimated using linear regression in the linear region with an estimate of 36 kPa.

#### **2.2.4 Friction Coefficient**

Friction tests were performed at room temperature because of concerns that the high temperature values would be extremely sensitive to degree of cure. The reported room temperature friction values were 0.19 for the tool-ply friction and 0.31 for the ply-ply friction.

#### **2.2.5 Summary of Mechanical Solvay CYCOM® 5320-1 prepreg Properties**

<b>Property</b>	<b>Value</b>
Tensile Modulus*	3.1 GPa
Flexural Modulus	9.7 MPa
In-Plane Shear Modulus	36 kPa
Tool-Ply Friction Coefficient*	0.19
Ply-Ply Friction Coefficient*	0.31

\*Values were measured at room temperature

##### **2.2.5.1 LS-DYNA material card calibration**

Material cards must be identified using an inverse analysis loop where the characterization test is performed virtually and the material parameters are adjusted according to some objective function, typically the sum of the squares of the distances between the model and experimental curves [10]. In this project, the J-composites preprocessor software was used to derive the material model.

Experimental conditions were designed in order to collect the most appropriate results for the material characterization in its ‘forming conditions’. By the time of the study, J-composites software (Figure 9) was the most efficient solution to automate the process of LS-Dyna material card model identification.

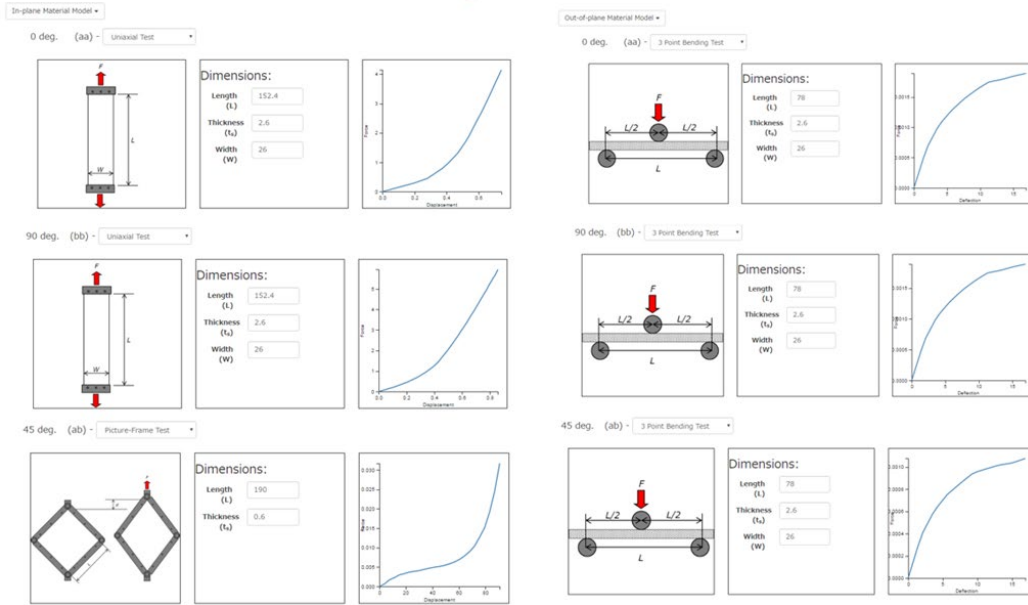


Figure 9. J-Composite preprocessing of experimental results for: Tensile (0, 90), Picture frame, 3 point bending (0,90, 45).

The picture frame was used for numerical correlation and calibration of the mesh dependency. Figure 10 represents a numerical and experimental correlation for Picture Frame test. The correlation shows a high level of accuracy and prediction for a flat simulation until the locking angle [5] [8] and it shows an accurate Material Card Model Characterization [3]. A similar approach was used for the bias extension test.

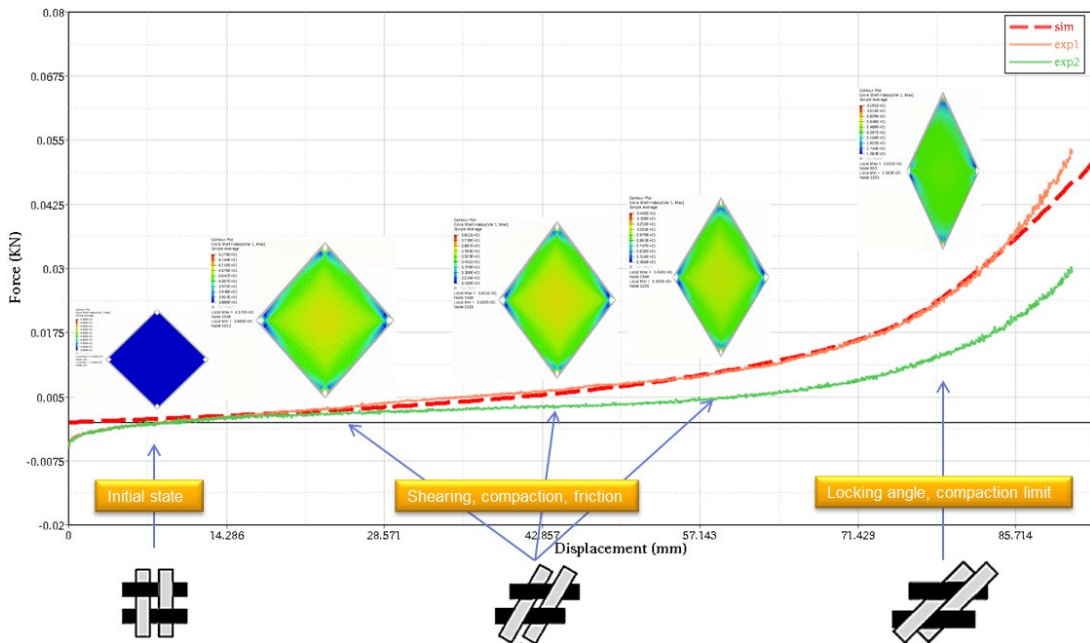


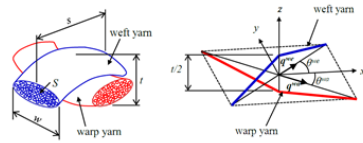
Figure 10. Picture frame test correlation between data and model used for the material cards

LS-Dyna MAT278 (Figure 11) was used for the press forming simulation presented in this article. This material model was developed for draping and curing analysis of pre-pregged woven carbon fibers; the model is a mixture of MAT234 & MAT277, where MAT234 provides the reorientation & locking phenomenon of fibers, while MAT277 provides the viscoelastic behavior of epoxy resin. The matrix resin along with the fiber orientation during deformation contribute to the overall stress state.

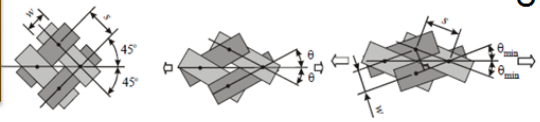
## MATERIAL MODEL

VARIABLE	DESCRIPTION	AREA	Fiber cross-sectional area.
MID	Material identification. A unique number or label not exceeding 8 characters must be specified.	APOT	Material axes option (see MAT_OPTIONTROPIC, ELASTIC for more complete description).
RO	Mass density.	VYARN	Volume fraction of yarn
E1	$E_p$ Young's modulus in the yarn axial-direction.	K1	Parameter $k_1$ for Kamal model.
E2	$E_p$ Young's modulus in the yarn transverse-direction.	K2	Parameter $k_2$ for Kamal model.
G12	$G_{12}$ Shear modulus of the yarns.	C1	Parameter $c_1$ for Kamal model.
G23	transverse shear modulus.	C2	Parameter $c_2$ for Kamal model.
EU	Ultimate strain at failure.	M	Exponent $m$ for Kamal model.
C	Coefficient of friction between the fibers.	N	Exponent $n$ for Kamal model.
EKA	Elastic constant of element "a".	CHEXP1	Quadratic parameter $\gamma_2$ for chemical shrinkage.
EUA	Ultimate strain of element "a".	CHEXP2	Linear parameter $\gamma_1$ for chemical shrinkage.
VMB	Damping coefficient of element "b".	CHEXP3	Constant parameter $\gamma_0$ for chemical shrinkage.
Ekb	Elastic constant of element "b".	LCCHEXP	Load curve ID to define the coefficient for chemical shrinkage $\gamma(a)$ as a function of the state of cure $a$ . If set, parameters CHEXP1, CHEXP2 and CHEXP3 are ignored.
THL	Yarn locking angle.	LCTHEXP	Load curve ID or table ID defining the instantaneous coefficient of thermal expansion $\beta(a, T)$ as a function of cure $a$ and temperature $T$ . If referring to a load curve, parameter $\beta(T)$ is a function of temperature $T$ .
TA	Transition angle to locking.	R	Gas constant $R$ for Kamal model.
THI1	Initial braid angle 1.	TREFEXP	Reference temperature $T_0$ for scant form of thermal expansion.
THI2	Initial braid angle 2.	XOCREFEXP	Reference degree of cure $a_0$ for sequential form of chemical expansion.
W	Fiber width.	WLTREF	Reference temperature for WLF shift function.
SPAN	Span between the fibers.	WLFA	Parameter $A$ for WLF shift function.
THICK	Real fiber thickness.	WLFB	Parameter $B$ for WLF shift function.
H	Effective fiber thickness.	LCG0	Load curve ID defining the instantaneous shear modulus $G_0$ as a function of state of cure.
		LCK0	Load curve ID defining the instantaneous bulk modulus $K_0$ as a function of state of cure.
		IDOC	Initial degree of cure.
		INCR	Switch between incremental and total stress formulation. EQ.0: total form: (DEFAULT) EQ.1: incremental form: (recommended)
		GI	Shear relaxation modulus for the $i$ th term for fully cured material.
		BETAGI	Shear decay constant for the $i$ th term for fully cured material.
		KI	Bulk relaxation modulus for the $i$ th term for fully cured material.
		BETAKI	Bulk decay constant for the $i$ th term for fully cured material.

Mat278=mat234+mat277



This is Material model developed for draping and curing analysis of prepreg. Is a mixture of two material models providing reorientation and locking phenomenon of fibers and providing the viscoelastic behavior of epoxy resin. Uses a micromechanical approach with linear viscoelastic elements connected by pin joint to rigid link elements



Card 1	1	2	3	4	5	6	7	8
Variable	MD	RO	E1	E2	G12	G23	EU	C
Type	A8	F	F	F	F	F	F	F

Card 2	1	2	3	4	5	6	7	8
Variable	EKA	EUA	VMB	EXB	THL	TA	THI1	THI2
Type	F	F	F	F	F	F	F	F

Card 3	1	2	3	4	5	6	7	8
Variable	W	SPAN	THICK	H	AREA			
Type	F	F	F	F	F			

Card 4	1	2	3	4	5	6	7	8
Variable	AOPT	A1	A2	A3				
Type		F	F	F				

Card 5	1	2	3	4	5	6	7	8
Variable	V1	V2	V3	D1	D2	D3		
Type	F	F	F	F	F	F		

Card 6	1	2	3	4	5	6	7	8
Variable	VYARN							
Type	F							

Card 6	1	2	3	4	5	6	7	8
Variable	K1	K2	C1	C2	M	N		
Type	F	F	F	F	F	F		

Card 7	1	2	3	4	5	6	7	8
Variable	EXP1	CHEXP2	CHEXP3	LCCHEX	LCTHEXP0	R	TREFEXP	ALPREFXP
Type	F	F	F	F	F	F	F	F

Card 8	1	2	3	4	5	6	7	8
Variable	WLTREF	WLFA	WLFB	LCG0	LCKBULK0	IDOC	XINORM	
Type	F	F	F	F	F	F	F	

Cure kinetics

Figure 11. LS-Dyna Material Card Definition.

## 3. RESULTS

The beaded panel and c-frame parts were simulated and performed in sequence one after the other. The results from the simulation are showed in the following sections.

### 3.1 Beaded Panel Geometry

The overall manufacturing simulation of the beaded panel is show in Figure 12. In the simulation, a blank is created and placed between two solid surfaces that represent the tool hard surfaces for matched metal tooling.

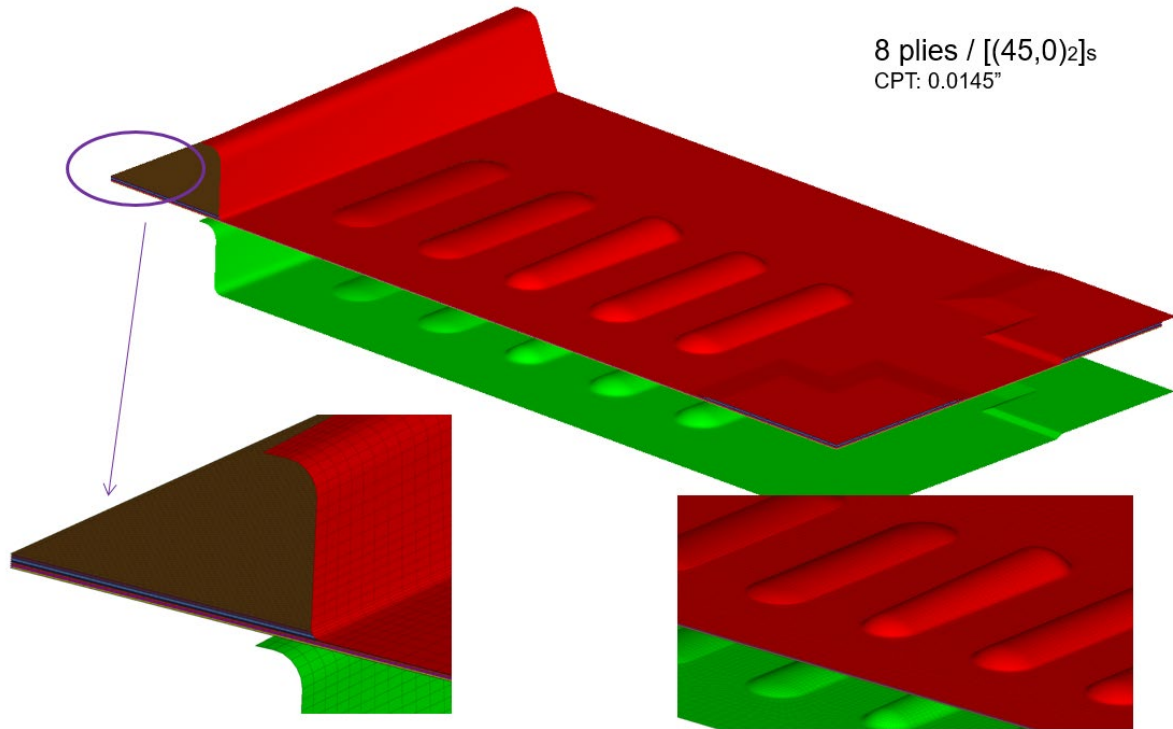


Figure 12. Beaded panel geometrical details.

Full laminate layup is simulated with multiple layers of shell elements built independently. Each mesh is aligned with a fiber direction, Figure 13. The Finite Element Model (FEM) included a mesh of 1.7 million elements and was simulated in 3h and 30 min using a computational system including 64 cores of 3.47GHz Intel Xeon processors [6] [9].

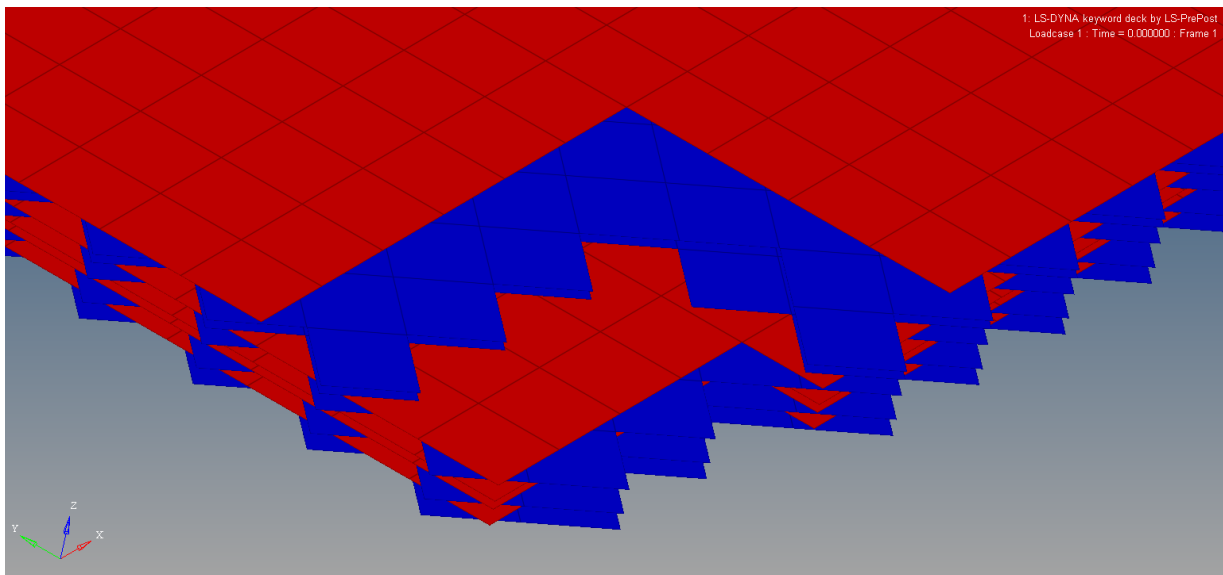


Figure 13. Multiple layers mesh dependency.

The post-processing result of the external layers is shown in the following Figures 14 and 15. The shear angle contour of ply 8 (a 45 degree ply) shows distortion lines at an angle deviation of 20.6 deg.

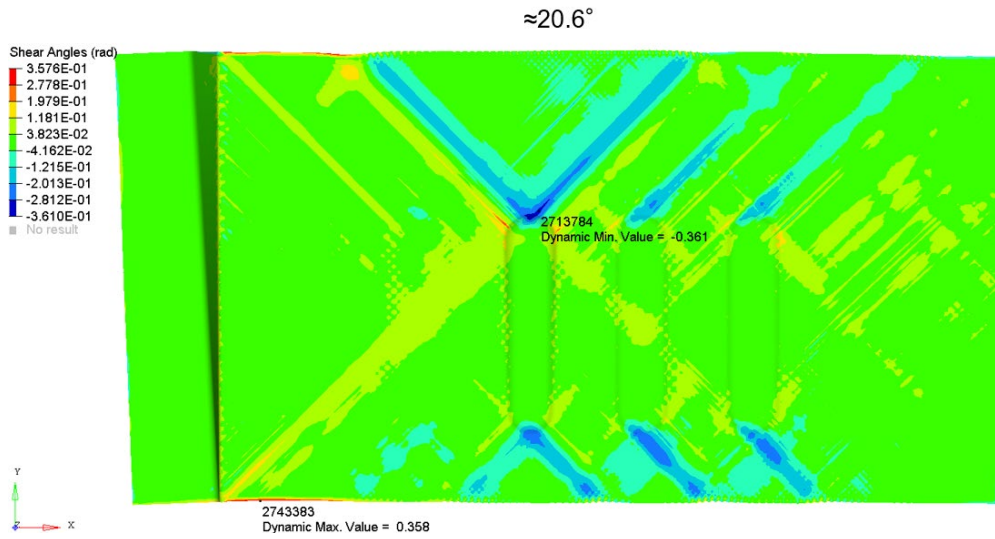


Figure 14. Shear angle deviation at ply 8 for the beaded panel geometry.

Figure 15 on the 0/90 degree ply 2 shows the global angle deviation is between 16.6 degrees to 18.9 degrees.

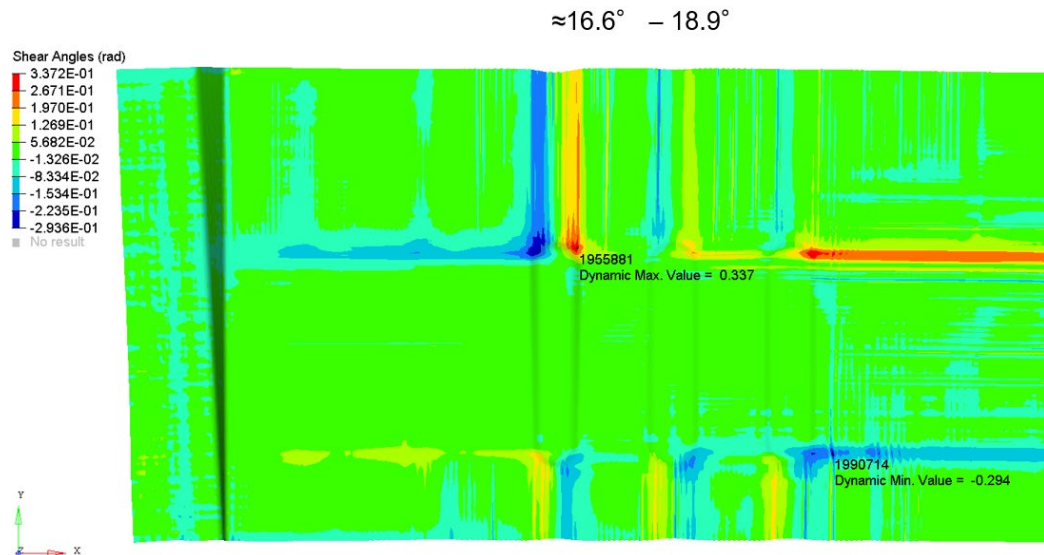


Figure 15. Shear angle fiber deviation at ply 2 for the beaded panel geometry.

In terms of correlation, a quick visual inspection was performed where a good correlation is found between the simulated and experimental part, as shown in Figure 16. As seen on the pictures, the

largest fiber deviation occurs on the center bead which corresponds to the larger out-of-plane geometrical feature (note: the center bead is intentionally higher on one end to test drape).

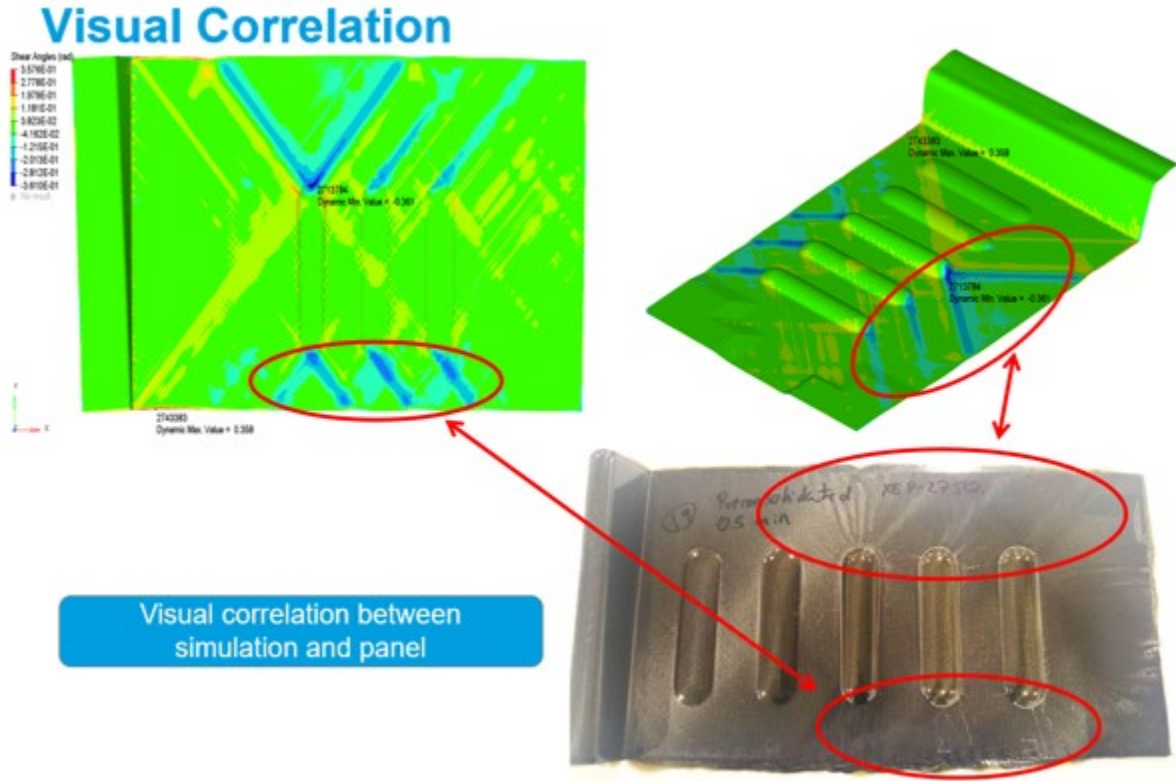


Figure 16. Visual and numerical correlation of fiber deviation between simulated and experimental results.

### 3.2 C-frame Geometry

The overall manufacturing set up for the C-channel component is shown in Figure 17. The model consisted in 33 plies, 34 contacts between plies, and 560,000 deformable elements. The model was run on 64 cores, 3.47 GHz CPU which yielded a simulation time of 7 hours. Just as in the previous geometry, the model consisted of two solid (metal) surfaces representing the tool with the 2D flat blank representation sandwiched between the surfaces at the beginning of the process. The flat blank is held by 10 springs distributed on the perimeter of the parts, 3 springs on each of the long sections and 2 springs on the narrow sections.

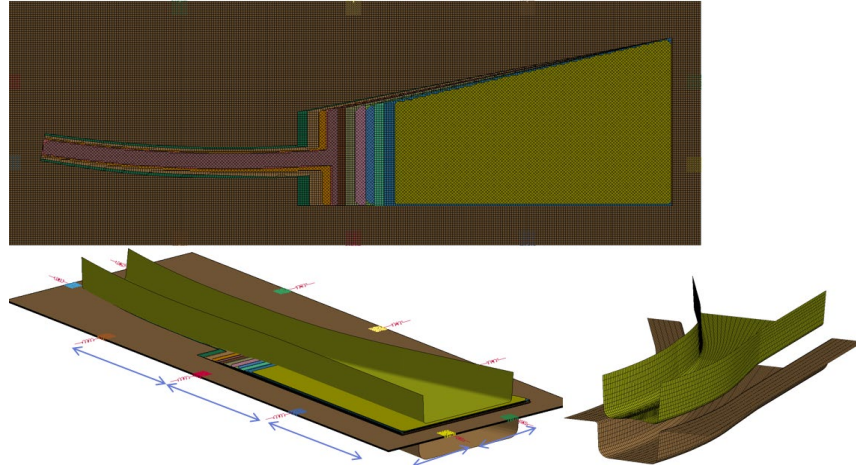


Figure 17. C-Frame simulation setup.

Figure 18 shows the simulation result after the forming process under specific spring boundary conditions. As seen in the Figure, the blank deforms to the desired tool shape with areas in the narrow section showing higher probability of wrinkling in the simulated setup. Estimated maximum fiber deviation for this geometry is 8 degrees.

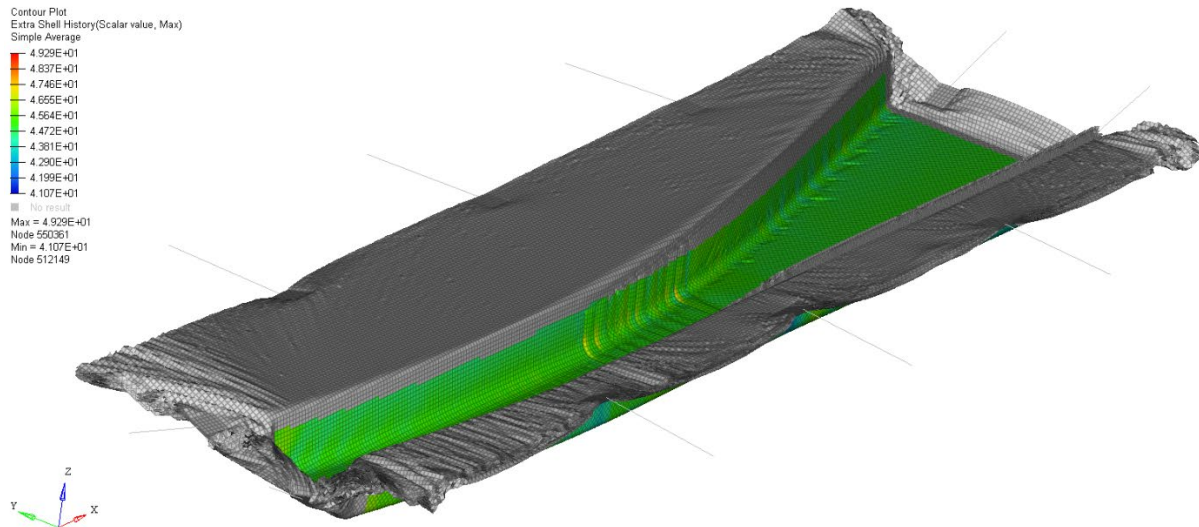


Figure 18. Results of the manufacturing simulation of the C-frame geometry.

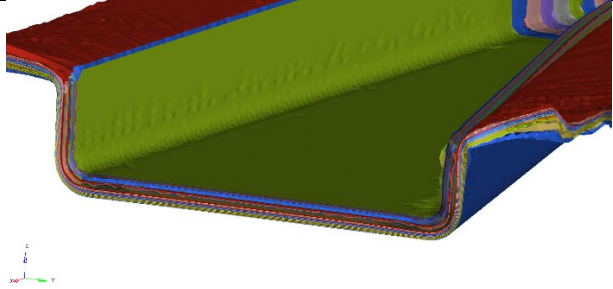
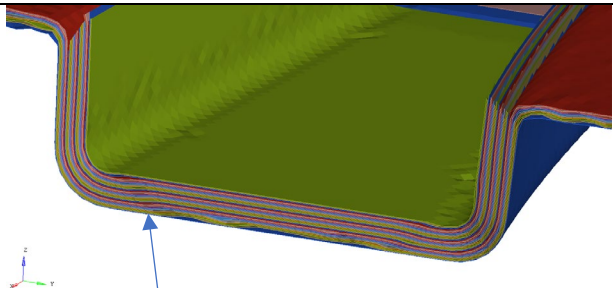
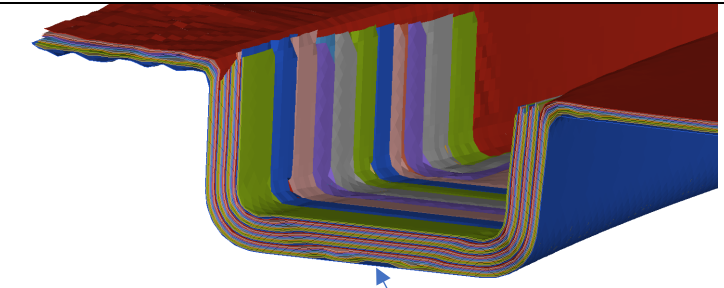
For this second geometry, the C-frame part, there are three important learnings and challenges:

1. Large & variable thicknesses are much more difficult to simulate and predict.
2. In the forming of multi-layered composites, out-of-plane wrinkling occurs due to the combination of intra-ply material deformations and inter-ply slippage.

3. The identification of the flat pattern of local reinforcements for large thickness was a complex procedure with an interactive trial and error process.

Table 1 shows the representation of different cross-sections of the part in different areas of the design. In a few sections of that part there are visible defects like wrinkling or compaction issues. Section (a) of the Table shows the area where high pressure in the internal curvature may generate potential thickness variations. In sections (b) and (c) show where potential for fiber deviation, wrinkling, and porosity increase due to the ply distortion as a result of manufacturing. Correlation between part manufacturing and numerical results were not available and is subject of future work.

*Table 1. Representation of different cross-sections of the part and potential for fiber deviation based on the current manufacturing simulation scenario.*

<p>a)</p> <p>High pressure in internal curvature</p> <p>Non-uniform thickness</p>	 <p>A 3D cross-sectional view of a curved, multi-layered part. The inner surface is highlighted in red, indicating high pressure. The thickness of the layers varies significantly, with some areas being much thicker than others. A small 3D coordinate system (X, Y, Z) is visible in the bottom left corner.</p>
<p>b)</p> <p>Fiber waviness</p> <p>Compaction issues / voids</p>	 <p>A 3D cross-sectional view of a curved, multi-layered part. The layers are shown with a wavy, distorted appearance, indicating fiber waviness. A blue arrow points to a specific area where the layers are compressed together, suggesting compaction issues or voids. A small 3D coordinate system (X, Y, Z) is visible in the bottom left corner.</p>
<p>c)</p> <p>Fiber waviness</p> <p>Compaction issues / voids</p>	 <p>A 3D cross-sectional view of a curved, multi-layered part. The layers are shown with a wavy, distorted appearance, indicating fiber waviness. A blue arrow points to a specific area where the layers are compressed together, suggesting compaction issues or voids. A small 3D coordinate system (X, Y, Z) is visible in the bottom left corner.</p>

## **4. CONCLUSIONS**

The proposed methodology of material modeling with the application of Ls-Dyna explicit numerical code is able to simulate the behavior of the fabric material. The simulations performed accounts for the fiber reorientation based on the material card developed. The fabric prepreg was characterized using a picture frame distortional test until the fiber locking angle was reached. The correlation was in good agreement with laboratory experiments.

The study of the beaded panel presented a good visual correlation between predicted fiber distortion in the forming simulation and the real composite part. This first simulation and correlation was used to identify the appropriate mesh density and the accuracy of the material card. Using the methodology developed for the first geometry, a second geometry was simulated and analyzed for fiber deviation. Both case scenarios show viability of the proposed approach by establishing the global simulation methodology. A more detailed correlation between numerical and experimental results is needed; this will be the focus of future work.

Simulation modeling of thermoset material is a great tool with a good visual correlation to actual parts. More development need to be done on correlation technologies like tomography and other scan methods. Another important future activity is developing a material card including methods to address viscosity and temperature dependency, especially for thermosets.

In conclusion, this work presents an efficient tool and methodology for predicting fiber direction, highlights potential fabric wrinkling, reduces tooling risk, and helps identify factors related to the press forming process for continuous fiber composite structures.

## **5. ACKNOWLEDGMENTS**

This effort was jointly accomplished by a Boeing-led team and the United States Government (Defense Advanced Research Projects Agency, DARPA) under the guidance of the United States Army Research Office, ARO. The authors would like to acknowledge the guidance and support of Dr. Jan Vandenbrande of DARPA/DSO and Dr. David Stepp of Army Research Office (ARO). The information in this paper was approved for public release by 19-162544-ETT and DISTAR 32485. Research was sponsored by the Defense Advanced Research Projects Agency (DARPA) and was accomplished under Cooperative Agreement Number W911NF-16-2-0087. The views and conclusions contained in this document are those of the authors and should not be interpreted as representing the official policies, either expressed or implied, of the Defense Advanced Research Projects Agency or the U.S. Government. The U.S. Government is authorized to reproduce and distribute reprints for Government purposes notwithstanding any copyright notation herein.

## **6. REFERENCES**

[1] Harrison, P., M. J. Clifford, and A. C. Long. "Shear characterization of viscous woven textile composites: a comparison between picture frame and bias extension experiments." *Composites Science and Technology* 64.10 (2004): 1453-1465.

- [2] Kenny, J. M., A. Apicella, and L. Nicolais. "A model for the thermal and chemo-rheological behavior of thermosets. I: Processing of epoxy-based composites." *Polymer Engineering & Science* 29.15 (1989): 973-983.
- [3] Zhang, Weizhao, Huaqing Ren, Biao Liang, Danielle Zeng, Xuming Su, Jeffrey Dahl, Mansour Mirdamadi, Qiangsheng Zhao, and Jian Cao. "A non-orthogonal material model of woven composites in the preforming process." *CIRP Annals* 66, no. 1 (2017): 257-260.
- [4] Liang, Biao, Nahiene Hamila, Mickaël Peillon, and Philippe Boisse. "Analysis of thermoplastic prepreg bending stiffness during manufacturing and of its influence on wrinkling simulations." *Composites Part A: Applied Science and Manufacturing* 67 (2014): 111-122.
- [5] Hamila, Nahiene, and Philippe Boisse. "Locking in simulation of composite reinforcement deformations. Analysis and treatment." *Composites Part A: Applied Science and Manufacturing* 53 (2013): 109-117.
- [6] Guzman-Maldonado, E., N. Hamila, P. Boisse, and J. Bikard. "Thermomechanical analysis, modelling and simulation of the forming of pre-impregnated thermoplastics composites." *Composites Part A: Applied Science and Manufacturing* 78 (2015): 211-222.
- [7] Guzman-Maldonado, E., N. Hamila, N. Naouar, G. Moulin, and P. Boisse. "Simulation of thermoplastic prepreg thermoforming based on a visco-hyperelastic model and a thermal homogenization." *Materials & Design* 93 (2016): 431-442.
- [8] Hamila, Nahiene, and Philippe Boisse. "Tension locking in finite-element analyses of textile composite reinforcement deformation." *Comptes Rendus Mécanique* 341, no. 6 (2013): 508-519.
- [9] Boisse, Philippe, Nahiene Hamila, Emmanuelle Vidal-Sallé, and François Dumont. "Simulation of wrinkling during textile composite reinforcement forming. Influence of tensile, in-plane shear and bending stiffnesses." *Composites Science and Technology* 71, no. 5 (2011): 683-692.
- [10] Nishi, Masato, and Tei Hirashima. "Forming simulation of textile composites using LS-DYNA." In *Proceedings of the 10th European LS-DYNA Conference, Würzburg, Germany*. 2015.
- [11] Schommer, Dominic, Miro Duhovic, and Joachim Hausmann. "Modeling of non-isothermal thermoforming of fabric reinforced thermoplastic composites." In *Proceedings 10th European LS-Dyna Conference*. 2015.
- [12] Luchini, T.J., Rodriguez, A.J., Rogers, S.A. Bras, A., Whysall, A., Russell, R., Lucas, S., and Hahn, G.L. "Spring Frame Press Fabrication of Aerospace Production Components." *SAMPE 2019 Conference Proceedings*. Charlotte, NC, May 20-23, 2019